Current Biology 21, 805–814, May 24, 2011 ©2011 Elsevier Ltd All rights reserved DOI 10.1016/j.cub.2011.04.016

Article

Sustained Elongation of Sperm Tail Promoted by Local Remodeling of Giant Mitochondria in *Drosophila*

Tatsuhiko Noguchi,[1] Michiko Koizumi,[1] and Shigeo Hayashi[1,2,*]

[1]Laboratory for Morphogenetic Signaling, RIKEN Center for Developmental Biology, 2-2-3 Minatojima-minamimachi, Chuo-ku, Kobe, Hyogo 650-0047, Japan

[2]Department of Biology, Kobe University Graduate School of Science, 1-1 Rokko-dai, Nada-ku, Kobe, Hyogo 657-8501, Japan

Summary

Background: Sperm length in Drosophilidae varies from a few hundred microns to 6 cm as a result of evolutionary selection. In postcopulatory competition, longer sperm have an advantage in positioning their head closer to the egg. Sperm cell elongation can proceed in the absence of an axoneme, suggesting that a mechanism besides intraflagellar transport emerged to sustain it.

Results: Here we report that sperm elongation in *Drosophila melanogaster* is driven by the interdependent extension of giant mitochondria and microtubule array that is formed around the mitochondrial surface. In primary cultures of elongating spermatids, we demonstrated that the mitochondrial integrity and local dynamics of microtubules at the tail tip region are essential for uniaxial elongation of the sperm tail. Mitochondria-microtubule linker protein Milton accumulated on mitochondria near the tail tip and is required for the sliding movement of microtubules. Disruption of Milton and its associated protein dMiro, and of potential microtubule crosslinkers Nebbish and Fascetto, caused strong elongation defects, indicating that mitochondria-microtubule association and microtubule crosslinking are required for spermatid tail elongation.

Conclusions: Mitochondria play unexpected roles in sperm tail elongation in *Drosophila* by providing a structural platform for microtubule reorganization to support the robust elongation taking place at the tip of the very long sperm tail. The identification of mitochondria as an organizer of cytoskeletal dynamics extends our understanding of mechanisms of cell morphogenesis.

Introduction

Diversity of sperm morphology has long been a source of fascination among reproductive biologists. This diversity evolved rapidly as a result of the intense postmating reproductive selection process called "sperm competition," in which sperm from different males compete for a chance to fertilize an egg. This selection has driven the evolution of sperm morphologies into unique shapes that maximize the opportunity for successful fertilization. Length of Drosophilidae sperm varies by up to two orders of magnitude [1], reaching 6 cm (over 20 times the male body length) in the extreme case of *Drosophila bifurca*. There is a strong correlation between the length of the sperm and that of the seminal receptacle, the female's sperm-storage organ [2], and a longer sperm tail may be advantageous for optimally positioning the sperm head for fertilization [3]. In addition, regional diversity in the sperm and storage organ can lead to morphological incompatibility, thereby promoting reproductive isolation and speciation [4, 5].

In the testis of *D. melanogaster*, right after meiosis, spherical spermatids of 10 μm in diameter, clustered in 64-cell cysts, elongate synchronously to become thin cylinders that are 0.6 μm in diameter and 1850 μm in length (Figure 1A). After elongation, each spermatid has lengthened 185-fold and increased its surface area 11-fold without increasing its volume ([6] and our own measurements), suggesting that elongation requires the construction of a very long internal skeleton and the production of an extensive membrane by the cell. There are four major structures running through the longitudinal axis of an elongating spermatid: the axoneme, cytoplasmic microtubules (MTs), mitochondria, and F-actin cables (Figures 1A–1G). Evidence suggests that the axoneme is dispensable for sperm elongation: spermatids can grow very long in axonemeless *Dsas-4* mutant flies [7] and also in mutants in which β2-tubulin isotype is replaced with a chimeric β2β3-hybrid tubulin [8]. Therefore, an axoneme-independent elongation mechanism is likely responsible for the extremely long sperm in Drosophilidae.

Insect sperm generally develop giant mitochondria that run along the length of the sperm tail [9, 10]. At the end of meiosis, a massive fusion of mitochondria mediated by Fuzzy onions, a testis-specific Mitofusin [11], leads to the two lobes of fused mitochondria being packed into a spherical structure called nebenkern [6]. During spermatid elongation, the mitochondrial lobes unfold and elongate parallel to the axoneme to fill the entire length of the tail. Hoyle and Raff speculated that it is these structures that extend the length of axonemeless mutant spermatids [8]. Here we report the interdependent role of the mitochondria and cytoplasmic MTs in sperm tail elongation, which highlights a novel role for mitochondria as an organizing center of MTs and cell morphogenesis.

Results

Elongation of the Spermatid In Vitro

In order to assess the contribution of the four longitudinal structures (axoneme, actin cables, cytoplasmic MTs, and mitochondria; Figures 1A–1G) in elongation, we used an in vitro culture system of spermatogenic cysts [12, 13] (Figure 1H; see also Movie S1 available online). Elongation speed of the cyst appeared to be fairly constant within a 12 hr time window (Figure 1I), although we did see a long-term increase from 0.39 ± 0.07 μm/min (first half, <1000 μm) to 0.70 ± 0.12 μm/min (second half, >1000 μm; wild-type [WT] in Figure 2D). Cyst length fluctuated in plots at higher time-space resolution (Figure 1I, inset), probably because of the winding and unwinding of a bundle of 64 spiral axonema within the cyst. Constant elongation is consistent with the anisotropic local elongation model, in which the elongation site is restricted to one area, and is inconsistent with the isotropic elongation model, which predicts an exponential increase in elongation speed (Figure 1J). We also confirmed that the

*Correspondence: shayashi@cdb.riken.jp

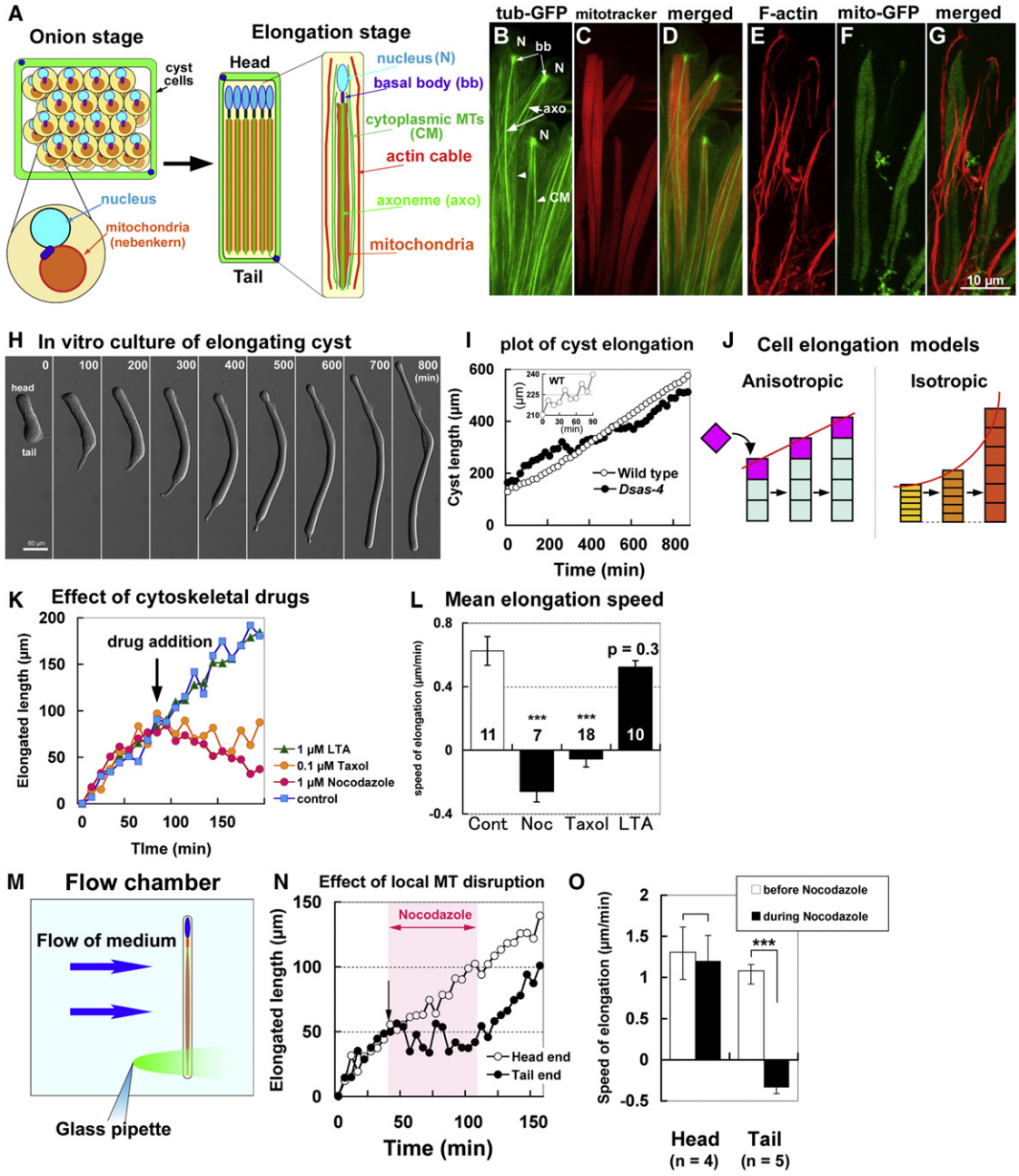

Figure 1. Spermatid Elongation In Vitro

(A) Schematic of spermatid development. After completion of meiosis (onion stage), 64 syncytial spermatids with giant mitochondrial derivatives (nebenkern) are formed in the spermatogenic cyst, enveloped by two somatic cyst cells, and elongate synchronously. Four major structures running through the length of the spermatid are indicated.

(B–D) MTs (green) and giant mitochondria (red) in elongating spermatids. The following abbreviations are used: axoneme, axo (arrows); cytoplasmic MT, CM (arrowheads); basal body, bb (small arrows); nucleus, N.

(E–G) F-actin cables (red) along longitudinal axis of the spermatids and mitochondria (green).

(H) Time-lapse series of an elongating cyst in vitro (Movie S1).

(I) Plot of wild-type and *Dsas-4*^{s2214} mutant cyst in early elongation. Inset is an enlarged plot of wild-type cyst elongation.

(J) Two models of cell elongation. Anisotropic model predicts a constant growth speed due to the growth occurring in a restricted area. Isotropic model predicts an exponential growth rate, with the growth occurring along the entire cell body.

(K) Pharmacological perturbation of cyst elongation at late stage (>1000 μm). Plot of cyst elongation is shown before and after adding latrunculin A (LTA), nocodazole (Noc), or taxol.

(L) Average elongation speed for the first 60 min in the presence of cytoskeletal drugs.

(M) A constant flow of culture medium was created in a flow chamber. Nocodazole solution (1 μM) was applied to one end cyst longer than 1200 μm.

(N) Plot of cyst elongation. Local treatment of nocodazole at the tail end of cyst reversibly inhibited elongation. Nocodazole treatment is in red.

(O) Mean elongation speed before and during the local nocodazole treatments. Sample numbers are on data bar (in L) or at the bottom (in O). Error bar represents standard error of the mean (SEM), two-tailed unpaired t test, ***$p < 0.001$.

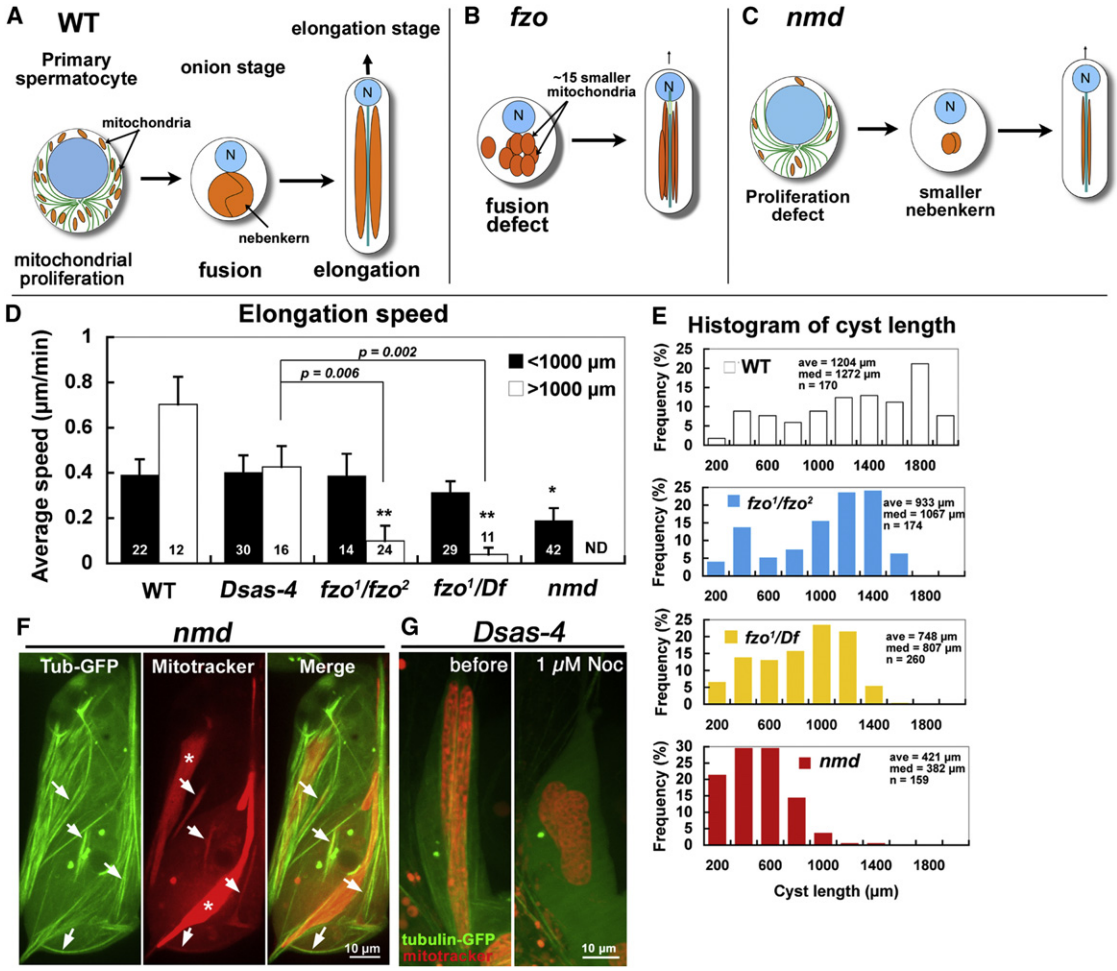

Figure 2. Mitochondria Are Essential for Elongation

(A–C) Schematic drawing for mitochondrial morphogenesis during spermatogenesis: wild-type (WT) (A), *fzo* mutant with smaller mitochondria because of defect in mitochondrial fusion (B), and *nmd* mutant with mitochondrial proliferation defect during primary spermatocytes (C).

(D) Elongation speed of WT, *Dsas-4* (axonemeless), *fzo*, and *nmd* mutant cysts. Cysts were classified into early (<1000 μm) and late (>1000 μm) stages, and their elongation speed was determined from time-lapse images taken for 60 min (unpaired two-tailed t test against speed of WT < 1000). Error bar represents SEM. *p < 0.05, **p < 0.01. Independently, a t test between *Dsas-4* (>1000 μm) and *fzo* (>1000 μm) mutants suggested that the size of the mitochondria had a more significant impact on the elongation process than complete loss of axoneme (sample numbers are on the data bars; p values are above the data bars; ND denotes no data).

(E) Cyst length distribution in five testes of each genotype.

(F) MT bundles (tubulin-GFP) formed around small mitochondria (red) in *nmd* mutant spermatid (arrows). * denotes large main mitochondria (still significantly smaller than normal).

(G) Morphology of giant mitochondria (red) in *Dsas-4* mutant during disruption of cytoplasmic MTs (green) by nocodazole.

axonemeless *Dsas-4* mutant spermatid could elongate to a significant length, although the very mild elongation defect suggests a supportive role of the axoneme in elongation (Figure 1I and Figure S1).

When MT function was disrupted by the MT-destabilizing drug nocodazole or the MT-stabilizing drug taxol, spermatid elongation was arrested, whereas the disruption of F-actin by latrunculin A had little or no effect on elongation (Figures 1K and 1L), suggesting that the elongation is dependent on MTs, but not on F-actin. Nocodazole treatment did not destroy the axoneme structure, which consists of stable MTs (see Figure 6). Application of nocodazole to a specific region of the spermatid using a flow chamber system (Figure 1M) locally inhibited the MT activity, as monitored by EB1-GFP (Figures S1H and S1I; Movie S2 and Movie S3). Inhibition of MTs at the tail region, but not at the head region, blocked the elongation of the entire cell in a reversible manner (Figures 1N and 1O), confirming that the elongation is localized and requires MT-based structures near the tail.

Size of Mitochondria Sets Limit to Spermatid Elongation

Next we examined the role of the fourth structure, giant mitochondria, which elongate from 6.5 μm to 1850 μm without an increase in organelle volume [6] (Figure 2A; Figure S2; Movie S4). A mutation in *fuzzy onions* (*fzo*) blocked mitochondrial fusion at the end of meiosis [11] and caused an obvious defect in elongation (Figures 2D and 2E). Length distribution of the cysts revealed that the population stopped elongating after peak value of 1400 μm in fzo^1/fzo^2 and 1200 μm in fzo^1/*deficiency chromosome* (*Df*) cells, compared to the peak value of 1800 μm in WT (Figure 2E), demonstrating that the second half of the elongation process was severely defective. This was in

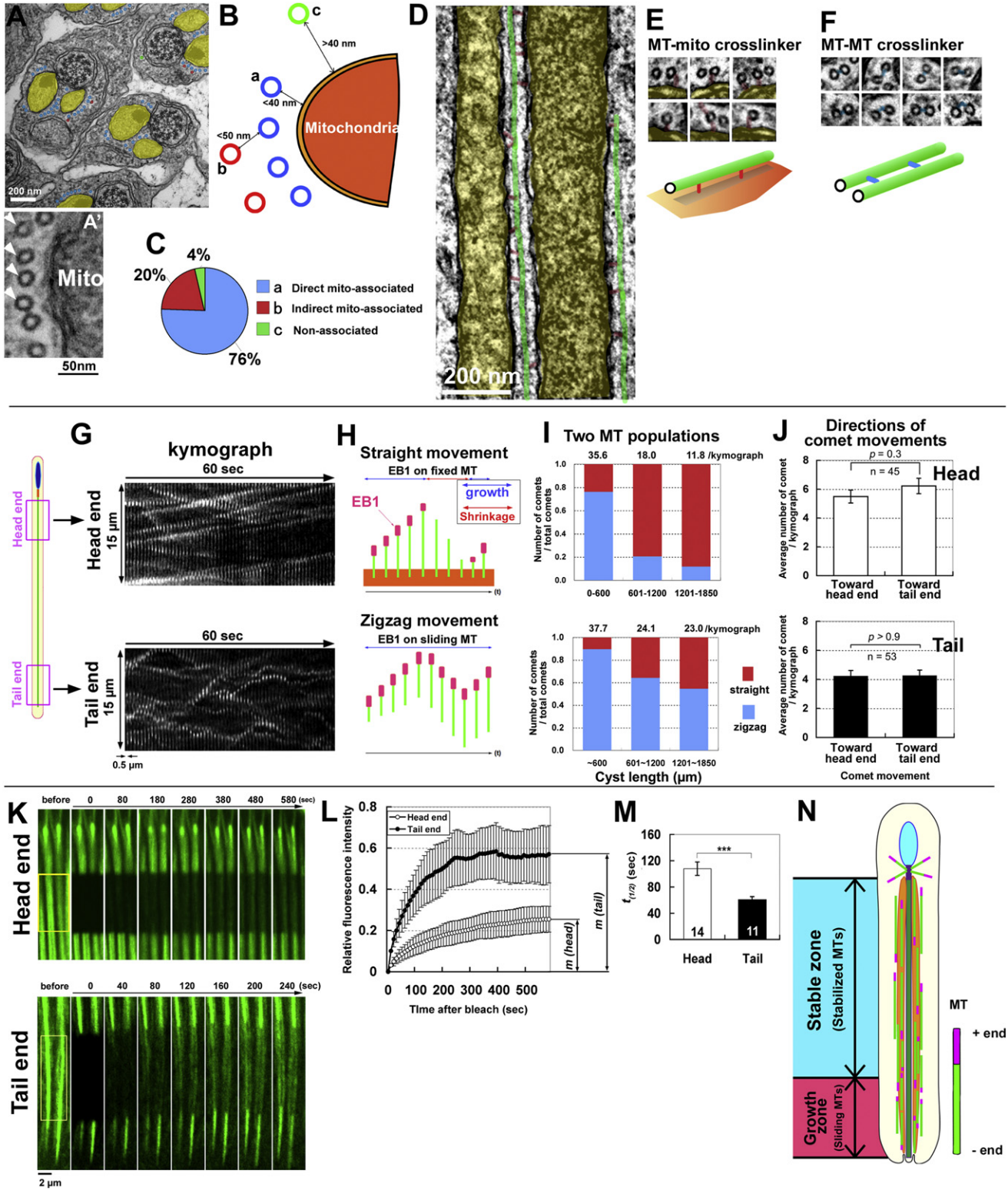

Figure 3. MT Array Organization near Head and Tail Ends

(A) EM cross-section of tail region of wild-type spermatids (mitochondria, yellow; MT, color-coded).

(A') Highly magnified view of cytoplasmic MTs (arrowheads) close to the mitochondrial surface.

(B) Classification of MTs based on distance from mitochondria. a denotes mitochondria-associated MT (blue) <40 nm from mitochondrial surface, b denotes indirectly associated MT (red) <50 nm from mitochondria-associating MT, and c denotes nonassociated MT (green).

(C) Pie graph of MT populations according to the categorization in (B).

(D) Longitudinal EM section of mitochondria (yellow) and associating MTs (green) with cross-bridges (red).

(E and F) Cross-sections of mitochondria-associating MTs.

contrast to the phenotype of axonemeless *Dsas-4* mutants, which maintained the same elongation rate throughout (Figure 2D). In *no mitochondrial derivative* (*nmd*; [14]) flies, which develop a much smaller nebenkern (Figure S2D), the spermatids showed a severe elongation defect (Figures 2D and 2E; Figure S2B). The mitochondrial membrane potential was normal in *fzo* mutants and only modestly reduced in *nmd* mutants (Figures S2D and S2E). These data suggest that it is the difference in mitochondrial size and morphology, and not the reduced mitochondrial respiratory activity, that is responsible for those observed defects in spermatid elongation.

Interestingly, in *nmd* mutants, arrays of cytoplasmic MTs formed around each of the small mitochondrion that took a highly elongated shape (Figure 2F). When the cytoplasmic MT array was destroyed by nocodazole in axonemeless *Dsas-4* mutants, the mitochondria immediately shrank back, suggesting that the elongation of mitochondria is dependent on associated cytoplasmic MTs (Figure 2G).

Cytoplasmic MT Array Mediates Mitochondrial Elongation

Electron microscopy (EM) images of cross-sections through the tail of elongating spermatids revealed that the vast majority of cytoplasmic MTs were located adjacent to mitochondria. Ninety-six percent of the MTs were considered "directly associated" with mitochondria or were considered "indirectly associated" when they were located in the vicinity of directly associated MTs (Figures 3A–3C; [15]). Cross- and longitudinal sections of elongating spermatids revealed connecting structures between the mitochondrial membrane and MTs, and also between the MTs themselves (Figures 3D–3F). These findings strongly suggest that MT array formation and mitochondria elongation are coupled by structural crosslinks.

Differential Regulation of MTs near the Tail End of Spermatids

To examine the orientation of cytoplasmic MTs, we expressed EB1-GFP in spermatids to identify and track the growing plus ends of the MTs [16] (Figure 3G and Movie S5). Time-lapse observation revealed three key features of cytoplasmic MT organization (Figure 3N). (1) Typical EB1-GFP comets (signals with comet-like shape and movement [16]) were distributed throughout the longitudinal axis of spermatids, suggesting that cytoplasmic MTs consist of short fragments [17]. (2) EB1-GFP signals moved in two distinct patterns (Figures 3G–3I). A kymograph of the head region shows straight diagonal lines (top panels), suggesting steady growth of MTs that are fixed to a solid support. In contrast, a kymograph of the tail end shows a zigzag pattern (bottom panels). Because EB1-GFP only labels growing MT plus ends [16], the zigzag pattern can be explained only by MTs sliding in the direction of their minus end (Figure 3H). During the early stage of elongation, most of the signals formed a zigzag pattern throughout the cyst. As the cyst elongated, a straight population became dominant near the head, whereas a zigzag movement persisted at the tail. Therefore, MT sliding was predominant in the tail region. The organization of MT arrays (Figures 3A–3F) suggests that MTs were either sliding over the mitochondrial surface or against neighboring MTs. (3) EB1-GFP signals moved in two directions along the axis of spermatids with equal frequency (Figure 3J).

To uncover the dynamics of the cytoplasmic MT array and its regional differences, we measured MT turnover using fluorescence recovery after photobleaching analysis of tubulin-GFP (Figures 3K–3M). MTs in the tail region recovered to a higher level (highly mobile fraction) with a faster recovery time ($t_{1/2}$) than in the head region, suggesting that turnover was more active in the tail.

Milton-dMiro Crosslink Mediates Mitochondrial Elongation and MT Sliding

The above results suggest that MT-mitochondria crosslinker and MT-MT crosslinker are involved in motor-driven sliding of MTs. We examined dynein and kinesin as candidate motors by making mutant clones in male germline cells (Figures 4A and 4B; Figure S3). *dynein* mutants showed severe chromosome segregation defects in meiosis (Figure S4), but these defective spermatids elongated normally. In contrast, *kinesin* mutants showed elongation defects in addition to defects occurring earlier than meiosis. To further pursue the possibility of kinesin's involvement, we next focused on known kinesin regulators in mitochondrial transport, Milton and dMiro, which act as a complex to link mitochondria and kinesin [18–20]. Previously, a mutation in *milton* was shown to delay mitochondrial elongation in the early stages of spermatid elongation [21]. dMiro, a regulator of Milton with two small GTPase domains, was also knocked down by RNA interference (RNAi). In both mutants, spermatid elongation was slowed and arrested prematurely (Figures 4C and 4D). To determine Milton localization, we expressed a GFP-fusion protein of the testis-specific isotype Milton-D [19] in male germline cells (Figures 4E–4M). From the onion stage to the early stage of elongation, GFP-Milton-D was localized uniformly on mitochondria. Later, it became concentrated in the tail-end region of the elongating spermatids. In $milt^{92}$ null mutant spermatids at the elongation stage, the tail end was abnormally thin, lacked mitochondria, and was sharply bent (Figures 4N and 4O, arrows). Similar defects were induced by RNAi knockdown of *milton* or *dmiro*, causing complete male sterility. Mitochondrial respiratory activity was normal in these mutants (Figures S2F and S2G). EM cross-sections showed that the axoneme was still present in the malformed tail region of *milton*-RNAi- or *dmiro*-RNAi-expressing spermatids, but the number and

(E) Mitochondria-MT crosslink (red).
(F) MT-MT crosslink (blue).
(G) Kymographs of EB1-GFP comets near the head and tail ends.
(H) Two patterns of EB1-GFP comet movement.
(I) Proportion of straight (red) and zigzag (blue) comet movements in the head and tail regions at three successive stages of elongation. The average number of comets/kymograph is depicted at the top of each data bar.
(J) MT orientation. Directions of straight-moving EB1-GFP comets were tracked from the kymographs. Error bar represents SEM; no statistical significance was detected between two populations with opposite orientation.
(K) Turnover of tubulin-GFP. Yellow rectangles in the "before" panels indicate photobleached area.
(L) Mean fluorescence recovery in the area was plotted. Error bar indicates standard deviation. The fluorescence recovery leveled off before reaching the original intensity, partly because mobile fraction (m) consists of cytoplasmic MTs. Nonexchangable axonemal tubulin is immobile.
(M) Rate of fluorescence recovery ($t_{1/2}$). Sample number is on the data bar. Error bar represents SEM, two-tailed unpaired t test, ***$p < 0.001$.
(N) Schematic summary for MT organization and dynamics in elongating spermatid.

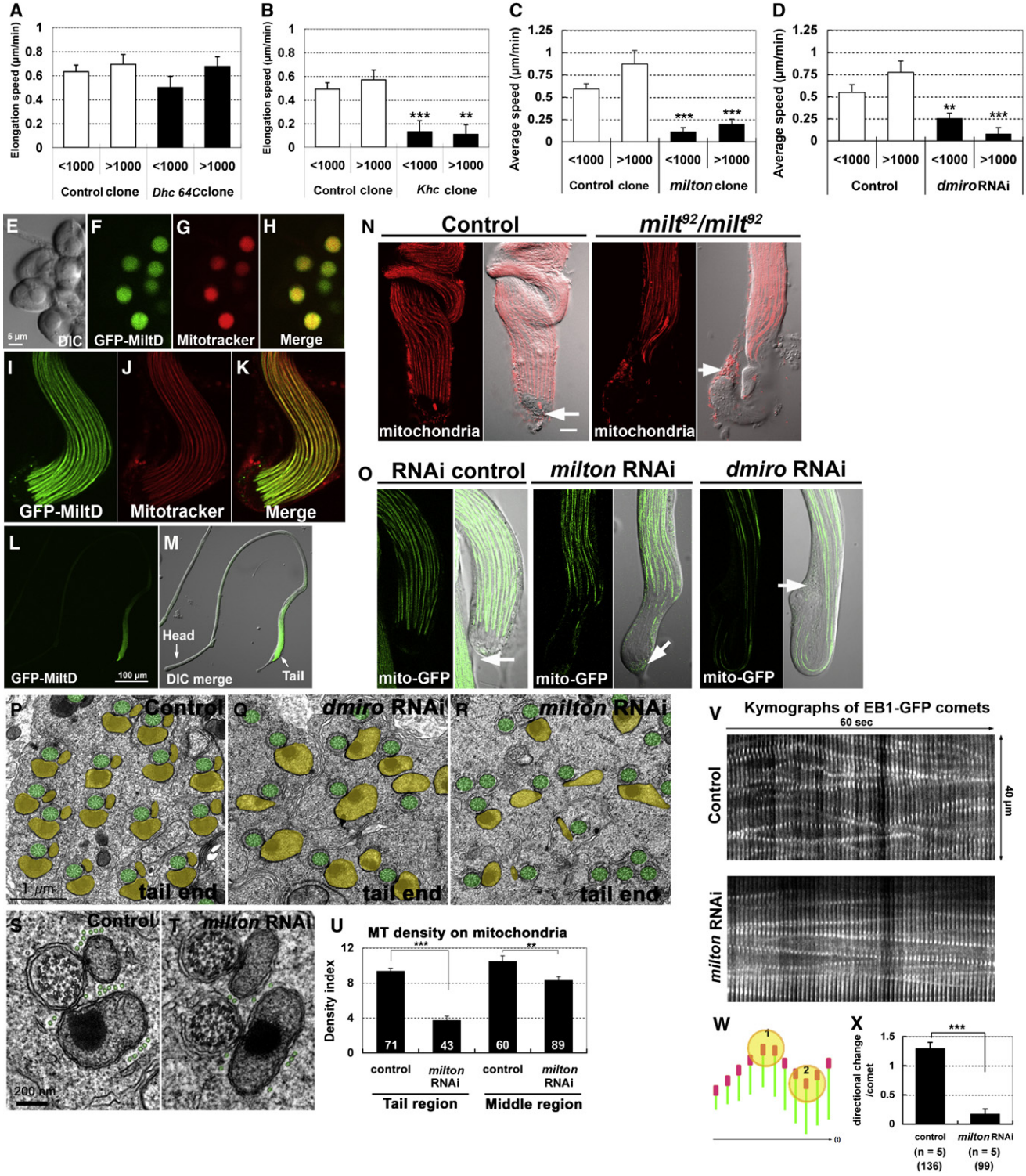

Figure 4. Localized Activity of Milton-dMiro Sustains Mitochondrial Elongation

(A–D) Elongation speed of Dhc $64C^{4-19}$ mutant clone (A), Khc^{23} mutant clone [33] (B), $milt^{92}$ mutant clone (C), and *dmiro* RNAi (D). Unpaired two-tailed t tests against control of <1000 μm length were performed.

(E–M) Localization of GFP-Milton-D on mitochondria (red) at onion stage (E–H) and at elongation stage (I–K).

(L and M) At later stages of elongation, concentration of GFP-Milton-D in the tail became intense.

(N and O) Tail-end morphology and mitochondria distribution in $milt^{92}$ mutant and *milton*/*dmiro* RNAi.

(N) Control and $milt^{92}$ mutant cysts stained with a mitochondrial marker (red) and merged DIC image.

(O) Control, *milton* RNAi, and *dmiro* RNAi cysts expressing Mito-GFP. Position of the tail tip is indicated by an arrow in each DIC panel.

(P–R) EM of cross-sections of control (P), *dmiro* RNAi (Q), and *milton* RNAi (R) elongating cysts. Sections were cut near the tail end, showing axoneme (green) and mitochondria (yellow).

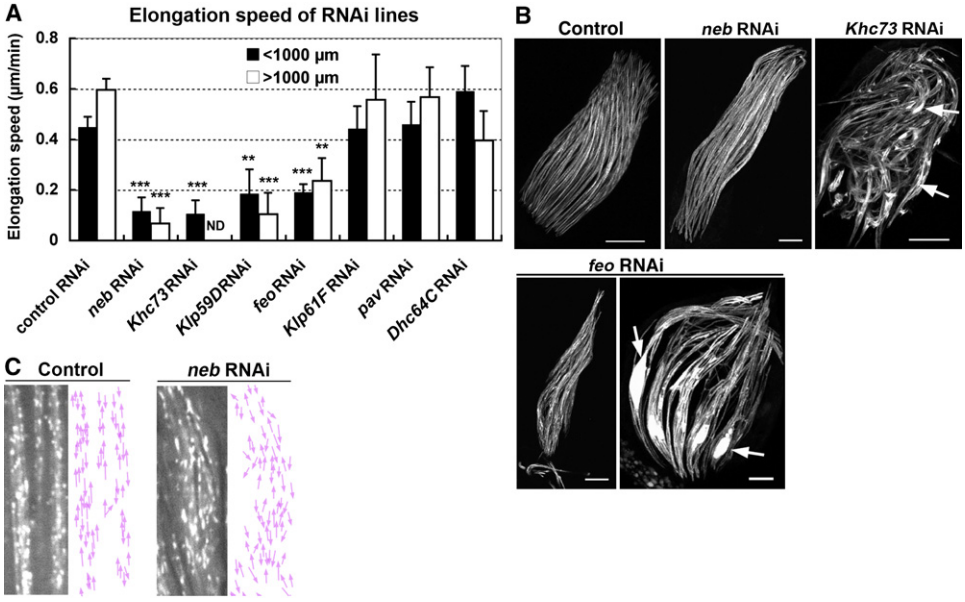

Figure 5. RNAi Analyses of MT Motors and MT Crosslinkers

(A) Elongation speed of cysts.

(B) Mitochondrial morphology in RNAi knockdown cysts. Mild and severe cases of *feo* RNAi are shown. Arrows indicate mitochondrial mass that failed to elongate.

(C) EB1-GFP comets (left) in elongating spermatid and their direction of movement (pink arrows on right) in control and *neb* RNAi lines. Note that orientations of comet movements were disorganized in *neb* RNAi line. ND denotes no data; error bar represents SEM. Unpaired two-tailed t tests against control were performed. $^{**}p < 0.01$, $^{***}p < 0.001$.

size of the mitochondria associated with the axoneme were significantly reduced (Figures 4P–4R). Density of MTs associated with the mitochondria was also greatly reduced in the tail region of *milton* RNAi spermatids (Figures 4S–4U). Kymographs of EB1-GFP comets in the thin tail region of *milton* RNAi knockdown revealed that MT sliding activity is greatly reduced, suggesting that a Milton-associating motor is required for the MT sliding activity near the tail (Figures 4V–4X). We speculate that other mitochondria-MT crosslinkers are involved, because some degree of spermatid elongation and fewer but significant numbers of MTs associated with mitochondria were observed when *milton/dmiro* was disrupted. Taken together, these data demonstrated that Milton and dMiro activities are required to attach MTs to the surface of mitochondria and to distribute mitochondria to the tail end of elongating spermatids. Furthermore, the bent shape of the spermatid tails that were devoid of mitochondria suggests that the remaining axoneme was insufficient to keep the spermatid tail straight, implying that mitochondria contribute to the structural support of the spermatid tail.

MT-MT Crosslinkers Are Required for Elongation and MT Array Formation

We further screened for MT motors and MT-MT crosslinkers required for spermatid elongation (Table S1). First, testes from the RNAi lines were observed to evaluate elongation. Second, elongation speed, cyst length, and mitochondrial morphology were examined. RNAi of *nebbish* (*neb*, a homolog of human KIF14 [22, 23]) showed strong elongation defects (Figure 5) [14]. Interestingly, the directions of EB1-GFP comet movements were no longer parallel to the longitudinal axis of the spermatid, suggesting that lateral MT-MT crosslinks were broken in *neb* RNAi lines (Figure 5C). Khc73, an MT bundler containing the MT plus-end-binding CAP-Gly domain and the motor domain [24], and Fascetto (Feo), an anti-parallel MT bundler (a *Drosophila* homolog of PRC1/Ase1 [25]), also showed elongation defects. In addition, Klp59D, a member of the MT depolymerizing kinesin-13 family [26], was required for elongation.

Formation of Cytoplasmic MTs at the Mitochondrial Surface

We noted that the MT arrays grew in the absence of a basal body, the classical MT organizing center (MTOC; Figure 6A). To identify the location of possible MT-organizing activity, we observed the site of MT regrowth after transient depolymerization by nocodazole (Figures 6B and 6C). Immediately, numerous speckles of tubulin-GFP emerged along the surface of mitochondria, suggesting that the mitochondria can form and organize an MT array around them. The spatial relationship of regrowing MT and mitochondria surface was further confirmed

(S and T) EM of spermatid cross-section near the tail end. Cross-sections of MTs are colored green.

(U) Density index of MTs associated with mitochondrial surface (number of MTs/μm of mitochondrial perimeter). Sample mitochondria number is shown on the data bar.

(V–X) MT sliding.

(V) Kymographs of EB1-GFP comet movement in tail end of cysts.

(W) Quantification of sliding activity by counting number of directional changes in comet movement. Two events are numbered 1 and 2 in yellow circles.

(X) Sliding activity in control and *milton* RNAi knockdown. n denotes number of kymographs examined. Total numbers of comets examined are at the bottom. Error bars in (A)–(D), (U), and (X) represent SEM. Unpaired two-tailed t tests against control were performed. $^{**}p < 0.01$, $^{***}p < 0.001$.

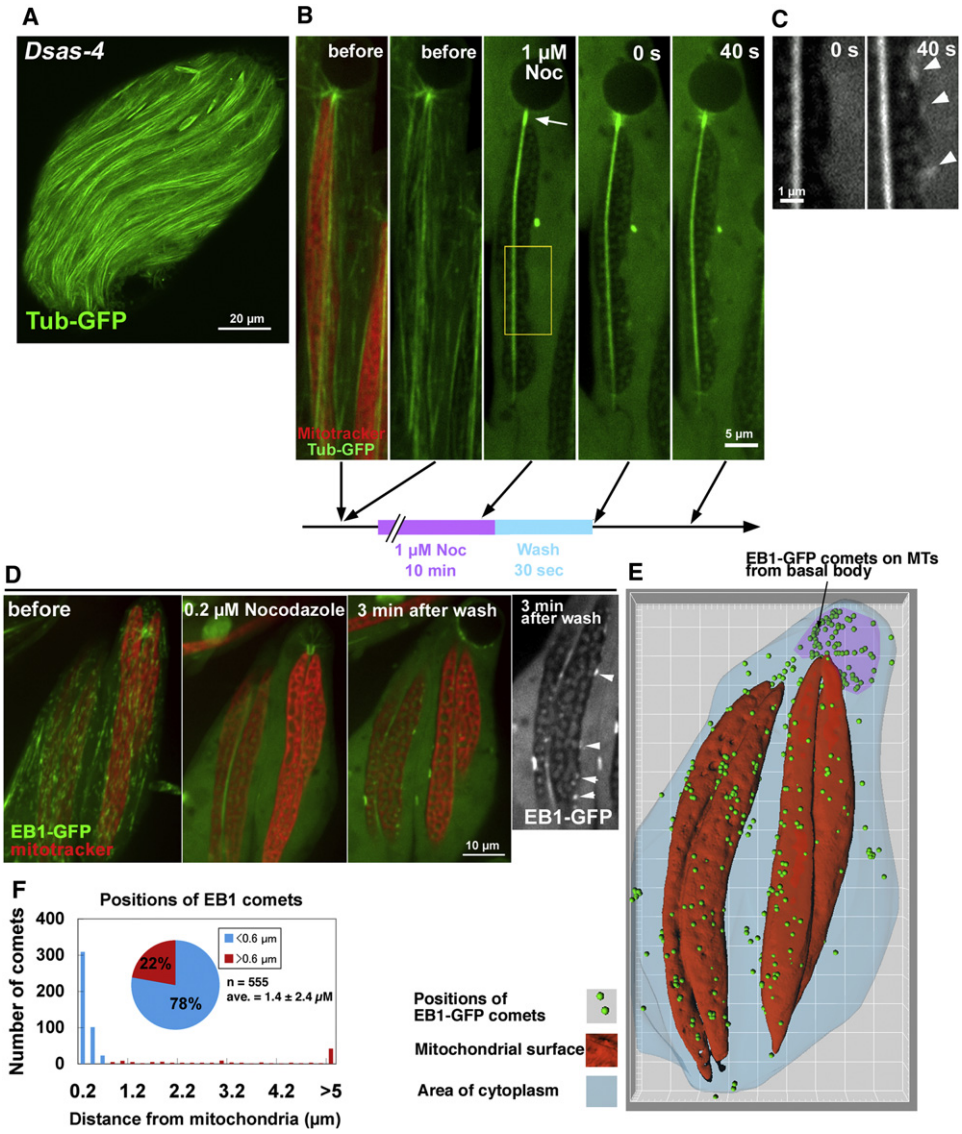

Figure 6. Mitochondria Serve as MT Organizing Centers

(A) Cytoplasmic MTs in axonemeless *Dsas-4* mutant.

(B) MT regrowth after a pulsed disruption by 1 μM nocodazole (Noc) in wild-type spermatid. The experimental procedure is summarized at the bottom of the panel. Dark areas are mitochondria devoid of unpolymerized tubulin-GFP signals. Basal body is indicated by an arrow.

(C) High-magnification view of mitochondrial surface of the boxed area in (B). Arrowheads indicate puncta of tubulin-GFP regrowing after nocodazole removal.

(D–F) Reappearance of EB1-GFP comets from the surface of mitochondria after pulsed treatment with nocodazole.

(D) EB1-GFP as a marker for regrowing MTs after nocodazole treatment. Puncta of EB1-GFP signal reappeared mainly around mitochondria. Rightmost panel shows EB1-GFP signal on the surface of mitochondria (arrowheads) at higher magnification. There are a few loci with relatively strong EB1 signals (see Figure S5).

(E) 3D rendering of mitochondria (red), center of EB1-GFP comet (green dots), and cytoplasmic area of two spermatids (light blue). Purple area indicates a nucleus.

(F) Distance distribution of EB1-GFP comets from the mitochondrial surface after pulse treatment of nocodazole.

by measuring the distance between the reappearing EB1-GFP signal and mitochondrial surface after 3D rendering, which revealed that 78% (433 of 555) of EB1-GFP spots were in close vicinity to the mitochondrial surface (Figures 6D–6F).

Discussion

We have shown here that the elongation of giant mitochondria, driven by the MT bundles associated with them, serves as a cell shape template during sperm tail elongation in *Drosophila melanogaster*. Because of their double-membrane architecture and large size, the giant mitochondria in *Drosophila* spermatids possess an intrinsic stiffness. Synchronizing the 64 pairs of mitochondrial elongation events in a cyst would greatly increase the overall strength of the spermatid bundle. When mitochondrial morphogenesis was impaired in *milton* mutants, the spermatids became bent, suggesting that the remaining axoneme was not physically strong enough

to support tail elongation. We therefore propose that the giant mitochondria are the main internal skeleton providing stiffness for elongating spermatid. This is the first report showing the determination of external cell morphology by mitochondria.

Acentrosomal mechanisms for continuous MT organization are observed in cells with long cytoplasmic extensions, such as neuronal axons [27], myotubes [28], root hair cells, and pollen tubes of plants [29]. Here we show that in the spermatid, mitochondria organize MTs independently from the classical MTOC (Figure 6). The coupling of cytoskeletal array formation with an energy-producing organelle would constitute a self-sustainable system for cell morphogenesis. The special context of the giant mitochondria in *Drosophila* spermatids may have allowed the Milton-dependent mitochondrial transport system to acquire a novel role in cell morphogenesis.

MT Motors and Crosslinkers Control Semistable MT-Mitochondria Interaction

This study revealed that three distinct regulations of MTs occur in the vicinity of the mitochondria: (1) new MT formation on the surface of mitochondria revealed by the MT regrowth experiment, (2) MT-mitochondria sliding mediated by MT-mitochondria crosslinker Milton/dMiro, and (3) lateral crosslinking of MTs mediated by kinesin family proteins encoded by *neb*, *Khc73*, and an antiparallel MT bundling protein encoded by *feo*. Through the combination of these three mechanisms, it is suggested that new MTs are formed and slide on the surface of mitochondria. Crosslinking of MTs in opposite orientations serves as a pivot point for extension or shrinkage of mitochondria when a motor protein complex crosslinking MTs and mitochondria generates a sliding force. Crosslinked parallel MTs slide together until their movement is slowed down by crosslinking to other MTs. Thus, as the number of crosslinked MTs increases, the MT array reaches a semistable tug-of-war situation, which is evident from the back-and-forth movement of EB1-GFP comets restricted within a few microns (Figure 3). Once a crosslinked MT network is established on the surface of mitochondria, it prevents the mitochondria from shrinking and functions as a ratchet, holding the mitochondria in an elongated shape.

Local Activation of MT Dynamics

Because spermatid elongation was sensitive to both MT-depolymerizing drug nocodazole and MT-stabilizing drug taxol and was also affected by RNAi of MT-depolymerizing kinesin Klp59D, a proper balance of MT polymerization and depolymerization is important for elongation (Figure 1 and Figure 5). The local drug application experiment demonstrated that MTs at the tail tip region are essential for elongation (Figure 1). Furthermore, accumulation of GFP-Milton-D and sliding and rapid turnover of MTs were limited to the tail tip region (Figure 3 and Figure 4), suggesting that MT-mitochondria crosslinking by a bound MT motor sustains MT sliding and growth zone. A similar relationship is seen during axon growth between dynamic MTs in the growth cone and the stable axonal MT bundle [30].

Model of Mitochondria-MT Array Elongation

Based on the MT array-mitochondria interaction described above, we propose a tentative model of spermatid elongation. At the tail region, the tip of elongating mitochondria provides an open surface for new MT formation. Crosslinking of antiparallel MTs stretches the mitochondria by sliding forces generated by the Milton-dMiro linker complex and exposes the membrane to create a new free surface for further MT formation and MT-mitochondria linkage. The crosslinked MTs develop into a network in a semistable tug-of-war state. Further crosslinking and slowing down of dynamics in the rear region ensure formation of highly stable MT arrays to maintain the elongated part of mitochondria. This interdependent feed-forward cycle ensures the continuous elongation of the MT array-mitochondria complex.

Evolution

How did sperm morphogenesis change so rapidly within a relatively short period of evolution? Switching from intraflagellar transport to a mitochondria-based elongation system may have facilitated the emergence of sperm-length variation. One key feature of the mitochondria-driven mechanism is that the elongation rate is determined by active mitochondrial remodeling at the tail tip region, marked by GFP-Milton-D. Variation in sperm length is also seen in Lepidoptera, in which it correlates with the size of the sperm-storage organ in the female [31]. The association of giant mitochondria with axoneme is a conserved characteristic of spermatids among insects, with some exceptions [11]. Thus, the sperm-elongation mechanism described in this report might be a general system for facilitating sperm-size variation among insects, thereby enhancing sexual selection and reproductive isolation.

Experimental Procedures

Live Imaging of Elongating Spermatids In Vitro

Primary culture of elongating spermatogenic cysts was performed as described previously [13]. The cultured cysts were fixed on a glass-bottomed dish (Iwaki) coated with poly-L-lysine (Sigma Diagnostics), and time-lapse differential interference contrast (DIC) images were recorded at 10 min intervals using an inverted microscope (Olympus IX-80) equipped with a 10× Plan-Apo lens and charge-coupled devise (CCD) camera (ORCA-2, Hamamatsu Photonics). Length of the cysts was measured using ImageJ (version 1.44) software. EB1-GFP comet movements were examined by a spinning disc confocal unit (CSU20, Yokogawa) and cooled CCD camera (ORCA-ER, Hamamatsu Photonics).

MT Regrowth Experiment

MTs and mitochondria were simultaneously visualized in real time with tubulin-GFP [32] and Mitotracker Red (25 nM, no cytotoxicity observed), respectively. Time series of dual-color images were recorded using CSU20. Treatment with 1 μM nocodazole for 10 min completely depolymerized MTs. The cysts were then washed five times with culture medium, and recovery of the MTs was monitored at 3 s intervals for 10 min.

Histogram of Elongating Cysts

Testes from five adult males were carefully dissected with glass needles to isolate all of the cysts and were then gently pipetted in culture medium to break up the clumps. DIC images of all of the elongating cysts were recorded, and the length of each cyst was measured using ImageJ software.

Local Drug Treatment of Elongating Spermatid

Relatively long cysts were selected for the recording to exclude any effects of drug treatment at the opposite end of the cyst. Nocodazole solution (1 μM) containing fluorescein isothiocianate-dextran (Invitrogen) was introduced into a restricted area of the cyst through a thin glass needle connected to a PicoPipet (Altair) under the constant flow of culture medium using a flow chamber.

Supplemental Information

Supplemental Information includes five figures, one table, Supplemental Experimental Procedures, and five movies and can be found with this article online at doi:10.1016/j.cub.2011.04.016.

Acknowledgments

The authors thank Y. Inoue, J.W. Raff, B. Saxton, K. Hales, T. Schwarz, K. Basler, K. Ohshima, Y. Yamashita, L. Tsuda, and M. Kaido for fly mutants and reagents and S. Yonemura and K. Misaki (RIKEN Center for Developmental Biology) for their expert advice on electron microscopy. We also thank the Drosophila Genetic Resource Center, the Bloomington Stock Center, and the Vienna Drosophila RNAi Stock Center for supplying fly lines. This work was supported by a Grant on the Priority Area "Systems Genomics" from the Ministry of Education, Culture, Sports, Science and Technology, Japan.

Received: July 15, 2010
Revised: February 22, 2011
Accepted: April 11, 2011
Published online: May 5, 2011

Reference

1. Pitnick, S., Markow, T.A., and Spicer, G.S. (1995). Delayed male maturity is a cost of producing large sperm in Drosophila. Proc. Natl. Acad. Sci. USA *92*, 10614–10618.
2. Pitnick, S., Markow, T., and Spicer, G.S. (1999). Evolution of multiple kinds of female sperm-storage organs in Drosophila. Evolution *53*, 1804–1822.
3. Pattarini, J.M., Starmer, W.T., Bjork, A., and Pitnick, S. (2006). Mechanisms underlying the sperm quality advantage in Drosophila melanogaster. Evolution *60*, 2064–2080.
4. Miller, G.T., and Pitnick, S. (2002). Sperm-female coevolution in Drosophila. Science *298*, 1230–1233.
5. Pitnick, S., Miller, G.T., Schneider, K., and Markow, T.A. (2003). Ejaculate-female coevolution in Drosophila mojavensis. Proc. Biol. Sci. *270*, 1507–1512.
6. Tokuyasu, K.T. (1975). Dynamics of spermiogenesis in Drosophila melanogaster. VI. Significance of "onion" nebenkern formation. J. Ultrastruct. Res. *53*, 93–112.
7. Basto, R., Lau, J., Vinogradova, T., Gardiol, A., Woods, C.G., Khodjakov, A., and Raff, J.W. (2006). Flies without centrioles. Cell *125*, 1375–1386.
8. Hoyle, H.D., and Raff, E.C. (1990). Two Drosophila beta tubulin isoforms are not functionally equivalent. J. Cell Biol. *111*, 1009–1026.
9. Phillips, D.M. (1970). Insect sperm: Their structure and morphogenesis. J. Cell Biol. *44*, 243–277.
10. Baccetti, B. (1998). Spermatozoa. In Microscopic Anatomy of Invertebrates: Insecta, *Volume 11C*, F.W. Harrison and M. Locke, eds. (New York: Wiley-Liss), pp. 843–894.
11. Hales, K.G., and Fuller, M.T. (1997). Developmentally regulated mitochondrial fusion mediated by a conserved, novel, predicted GTPase. Cell *90*, 121–129.
12. Cross, D.P., and Shellenbarger, D.L. (1979). The dynamics of Drosophila melanogaster spermatogenesis in in vitro cultures. J. Embryol. Exp. Morphol. *53*, 345–351.
13. Noguchi, T., and Miller, K.G. (2003). A role for actin dynamics in individualization during spermatogenesis in Drosophila melanogaster. Development *130*, 1805–1816.
14. Fuller, M.T. (1993). Spermatogenesis. In The Development of *Drosophila melanogaster*, *Volume 1*, M. Bate and A.M. Arias, eds. (New York: Cold Spring Harbor Laboratory Press), pp. 71–147.
15. Tokuyasu, K.T. (1974). Dynamics of spermiogenesis in Drosophila melanogaster. 3. Relation between axoneme and mitochondrial derivatives. Exp. Cell Res. *84*, 239–250.
16. Mimori-Kiyosue, Y., Shiina, N., and Tsukita, S. (2000). The dynamic behavior of the APC-binding protein EB1 on the distal ends of microtubules. Curr. Biol. *10*, 865–868.
17. Lindsley, D.L., and Tokuyasu, K.T. (1980). Spermatogenesis. In Genetics and Biology of *Drosophila*, Second Edition, M. Ashburner and T.R. Wright, eds. (New York: Academic Press), pp. 225–294.
18. Stowers, R.S., Megeath, L.J., Górska-Andrzejak, J., Meinertzhagen, I.A., and Schwarz, T.L. (2002). Axonal transport of mitochondria to synapses depends on milton, a novel Drosophila protein. Neuron *36*, 1063–1077.
19. Glater, E.E., Megeath, L.J., Stowers, R.S., and Schwarz, T.L. (2006). Axonal transport of mitochondria requires milton to recruit kinesin heavy chain and is light chain independent. J. Cell Biol. *173*, 545–557.
20. Guo, X., Macleod, G.T., Wellington, A., Hu, F., Panchumarthi, S., Schoenfield, M., Marin, L., Charlton, M.P., Atwood, H.L., and Zinsmaier, K.E. (2005). The GTPase dMiro is required for axonal transport of mitochondria to Drosophila synapses. Neuron *47*, 379–393.
21. Aldridge, A.C., Benson, L.P., Siegenthaler, M.M., Whigham, B.T., Stowers, R.S., and Hales, K.G. (2007). Roles for Drp1, a dynamin-related protein, and milton, a kinesin-associated protein, in mitochondrial segregation, unfurling and elongation during Drosophila spermatogenesis. Fly (Austin) *1*, 38–46.
22. Molina, I., Baars, S., Brill, J.A., Hales, K.G., Fuller, M.T., and Ripoll, P. (1997). A chromatin-associated kinesin-related protein required for normal mitotic chromosome segregation in Drosophila. J. Cell Biol. *139*, 1361–1371.
23. Gruneberg, U., Neef, R., Li, X., Chan, E.H., Chalamalasetty, R.B., Nigg, E.A., and Barr, F.A. (2006). KIF14 and citron kinase act together to promote efficient cytokinesis. J. Cell Biol. *172*, 363–372.
24. Siegrist, S.E., and Doe, C.Q. (2005). Microtubule-induced Pins/Galphai cortical polarity in Drosophila neuroblasts. Cell *123*, 1323–1335.
25. Vernì, F., Somma, M.P., Gunsalus, K.C., Bonaccorsi, S., Belloni, G., Goldberg, M.L., and Gatti, M. (2004). Feo, the Drosophila homolog of PRC1, is required for central-spindle formation and cytokinesis. Curr. Biol. *14*, 1569–1575.
26. Rath, U., Rogers, G.C., Tan, D., Gomez-Ferreria, M.A., Buster, D.W., Sosa, H.J., and Sharp, D.J. (2009). The Drosophila kinesin-13, KLP59D, impacts Pacman- and Flux-based chromosome movement. Mol. Biol. Cell *20*, 4696–4705.
27. Stiess, M., Maghelli, N., Kapitein, L.C., Gomis-Rüth, S., Wilsch-Bräuninger, M., Hoogenraad, C.C., Tolić-Nørrelykke, I.M., and Bradke, F. (2010). Axon extension occurs independently of centrosomal microtubule nucleation. Science *327*, 704–707.
28. Tassin, A.M., Maro, B., and Bornens, M. (1985). Fate of microtubule-organizing centers during myogenesis in vitro. J. Cell Biol. *100*, 35–46.
29. Hepler, P.K., Vidali, L., and Cheung, A.Y. (2001). Polarized cell growth in higher plants. Annu. Rev. Cell Dev. Biol. *17*, 159–187.
30. Tanaka, E., Ho, T., and Kirschner, M.W. (1995). The role of microtubule dynamics in growth cone motility and axonal growth. J. Cell Biol. *128*, 139–155.
31. Morrow, E.H., and Gage, M.J. (2000). The evolution of sperm length in moths. Proc. Biol. Sci. *267*, 307–313.
32. Inoue, Y.H., Savoian, M.S., Suzuki, T., Máthé, E., Yamamoto, M.T., and Glover, D.M. (2004). Mutations in orbit/mast reveal that the central spindle is comprised of two microtubule populations, those that initiate cleavage and those that propagate furrow ingression. J. Cell Biol. *166*, 49–60.
33. Brendza, K.M., Rose, D.J., Gilbert, S.P., and Saxton, W.M. (1999). Lethal kinesin mutations reveal amino acids important for ATPase activation and structural coupling. J. Biol. Chem. *274*, 31506–31514.